metals

MDPI

Article

Effect of Electro-Pulse on Microstructure of Al-Cu-Mn-Zr-V Alloy during Aging Treatment and Mechanism Analysis

Dequan Shi [1], Wenbo Yu [1], Guili Gao [2,*] and Kaijiao Kang [3,*]

[1] School of Materials and Chemistry, University of Shanghai for Science and Technology, Shanghai 200093, China
[2] School of Mechanical and Energy Engineering, Shanghai Technical Institute of Electronics and Information, Shanghai 201411, China
[3] School of Materials Science & Chemical Engineering, Harbin University of Science and Technology, Harbin 150080, China
* Correspondence: gao-guili@163.com (G.G.); kangkaijiao92@163.com (K.K.)

Abstract: The effects of electro-pulse on microstructure and mechanical properties of Al-Cu-Mn-Zr-V alloy were investigated, and the ageing mechanism was analyzed. As the current density increases, the size and quantity of precipitates gradually transit from continuous aggregation to dispersion at grain boundaries, and the mechanical properties are improved. When the current density is 15 A·mm^{-2}, the precipitates are smallest and the mechanical properties are best. The tensile strength is 443.5 MPa and the elongation is 8.1%, which are 51.7% and 42.1% higher than those of conventional ageing treatment, respectively. Once the current density exceeds 15 A·mm^{-2}, the precipitates will increase again and gather at grain boundaries, and the mechanical properties also decrease. An additional electrical free energy arising from an electro-pulse provides thermodynamic and kinetic conditions for the ageing precipitation of second phases. The electro-pulse can enhance the ageing diffusion coefficient, being improved by 34 times for 15 A·mm^{-2}. The electro-pulse improves the nucleation rate and decreases the critical nucleation radii of second phases. However, it also accelerates the grain growth, making the second phases become coarse. An electro-pulse with a current density of 15 A·mm^{-2} can rapidly nucleate the second phase at 463 K while the precipitates are relatively small after growth.

Keywords: electro-pulse; current density; ageing treatment; Al-Cu-Mn-Zr-V alloy; mechanical properties; mechanism analysis

check for updates

Citation: Shi, D.; Yu, W.; Gao, G.; Kang, K. Effect of Electro-Pulse on Microstructure of Al-Cu-Mn-Zr-V Alloy during Aging Treatment and Mechanism Analysis. *Metals* **2024**, *14*, 648. https://doi.org/10.3390/met14060648

Academic Editor: Martin Heilmaier

Received: 26 April 2024
Revised: 25 May 2024
Accepted: 27 May 2024
Published: 29 May 2024

Copyright: © 2024 by the authors. Licensee MDPI, Basel, Switzerland. This article is an open access article distributed under the terms and conditions of the Creative Commons Attribution (CC BY) license (https://creativecommons.org/licenses/by/4.0/).

1. Introduction

Al-Cu alloy is one of the representative high-strength cast aluminum alloys, which has excellent mechanical properties and has been widely used in the fields of aerospace, defense, and civil tools [1,2]. The addition of alloying elements such as Mn, Zr, V, and Ti can significantly improve the thermal stability, high-temperature performance, and corrosion resistance of Al-Cu alloys [3–5]. The mechanical properties of Al-Cu-X serials cast aluminum alloy can be greatly improved by the heat treatment [6]. However, there is still a problem of slow speed of heat treatment [7]. Accordingly, there is a need to develop a new process for improving conventional heat treatment and thus promoting the comprehensive performances of high-strength cast aluminum alloys.

In recent years, some studies have been conducted on the method of adopting electro-pulse to improve the microstructure and mechanical properties [8]. According to these research results, the electro-pulse applied in the solidification process of aluminum alloys can break dendrites, promote uneven nucleation of metals, reduce grain size, and so on [9,10]. For the ageing treatment, the electro-pulse can not only improve microstructure and mechanical properties of the alloys, but also reduce the heat treatment time. Liu et al. [11] concluded that the low-density pulse current can promote the ageing precipitation,

shorten the ageing time, and make precipitates more dispersive for AA2219 alloy. Chen et al. [12] found the elongation of 7075 alloy can be improved significantly by 6.7% at a frequency of 200 Hz while the tensile strength changes slightly, which is attributed to the fact that the electric pulse changes the number and distribution of the second phase precipitations. Bian et al. [13] synchronously applied an electrical pulse with a frequency of 300 Hz and a current density of 15 A·mm^{-2} to the steady-state creep aging of Al-Zn-Mg-Cu alloy; the hardness and corrosion resistance of alloy were improved and were higher than those of conventional creep ageing. Kang et al. [14] concluded that the ageing time can be shortened by 12 h when an electric pulse is used for the ageing treatment of Al-Zn-Mg-Cu alloy, and the tensile strength and elongation are 14.1 MPa and 4.45% higher than that of conventional heat treatment, respectively. However, there is little research on the influence and mechanism of electro-pulse parameters on the ageing treatment of Al-Cu-Mn-Zr-V alloy.

In this study, the conventional ageing (CA) treatment and the ageing treatment with electro-pulse (AEP) were performed on the samples of Al-Cu-Mn-Zr-V cast aluminum alloy, respectively. The purpose is to investigate the feasibility of electro-pulse-assisted ageing treatment for Al-Cu-Mn-Zr-V alloy in order to reduce the ageing time and/or improve the mechanical properties of the alloy.

2. Materials and Methods

The Al-Cu-Mn-Zr-V cast aluminum alloy was prepared by pouring alloy liquid into a metal mold, and the actual chemical composition of alloy is shown in Table 1, which is consistent with the actual industrial production. The structure and size of samples for ageing treatment are shown in Figure 1.

Table 1. Chemical compositions of Al-Cu-Mn-Zr-V alloy.

Element	Cu	Mn	Zr	V	Ti	Fe	Si	Al
Content (wt.%)	5.02	0.33	0.15	0.11	0.09	0.04	0.01	Bal.

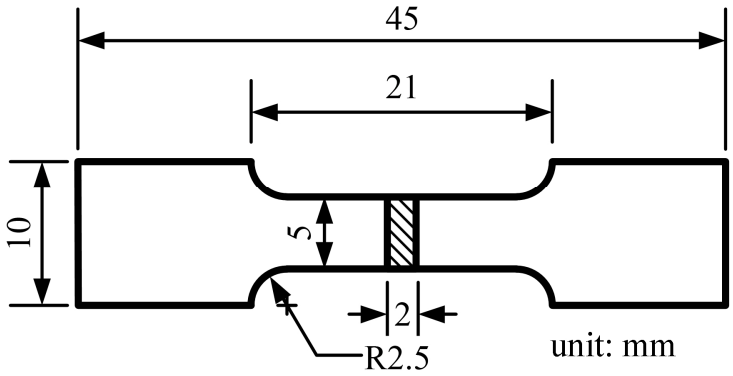


Figure 1. Sample size of Al-Cu-Mn-Zr-V alloy.

In order to design preferably the solid solution temperature, a differential scanning calorimeter (METTLER DSC3+, Zurich, Switzerland) was adopted to measure the DSC curve of the alloy, with a heating rate of 10 °C·min^{-1} and a shielding gas of argon. As shown in Figure 2, the DSC curve expresses that the temperature corresponding to the endothermic peak is 549.5 °C, at which the eutectic phase is melted for Al-Cu-Mn-Zr-V alloy. Considering that the solid solution temperature should be 15–30 °C lower than the eutectic melting temperature, it is determined to be 530 °C.

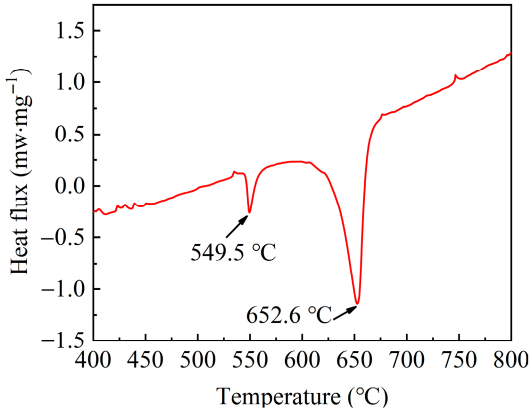


Figure 2. DSC curve of Al-Cu-Mn-Zr-V alloy.

Therefore, the heat treatment process for Al-Cu-Mn-Zr-V alloy is as follows. First, a secondary solid solution treatment, including first solid solution temperature of 495 ± 5 °C and the holding time of 5 ± 0.5 h, and second solid solution temperature of 530 ± 5 °C and the holding time of 24 ± 0.5 h, was conducted on the samples. Second, the samples were immediately transferred into water for quenching at temperature of 65 ± 2 °C. Then, the ageing treatment at 190 ± 2 °C and 26 ± 0.5 h (the ageing parameters are determined by the actual industrial production of Al-Cu-Mn-Zr-V alloy) was conducted in an ageing furnace. When the ageing furnace temperature had risen to 190 °C, the electro-pulse with different current density was applied to the samples for 10 s every 5 min until the end of ageing. Finally, the samples were cooled to room temperature.

The principal diagram of ageing treatment with electro-pulse is shown in Figure 3. In order to prevent the Joule heat generated by the electro-pulse, the electro-pulse with different current density was applied to the samples at room temperature, and the temperature of samples was monitored by the thermocouple attached to the sample surface. The current density causing the temperature rise of 2 °C is taken as the maximum, and the experiments indicated the maximum current density is 28.5 A·mm^{-2}. Accordingly, the scheme of the ageing treatment with electro-pulse is shown in Table 2 where three samples were carried out for each experiment.

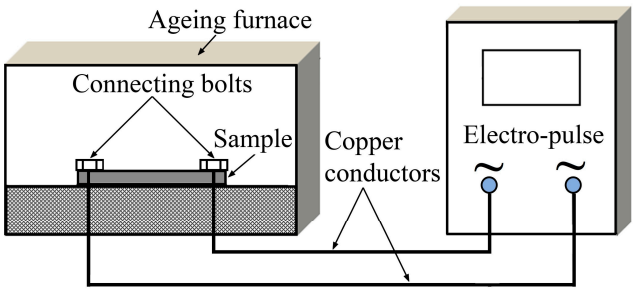


Figure 3. Principal diagram of ageing treatment with electro-pulse.

Table 2. The parameters of electro-pulse used for ageing treatment.

No.	Current Density (A·mm^{-2})	Duty Ratio (%)	Frequency (Hz)
1	0	0	0
2	5	1	100
3	10	1	100
4	15	1	100
5	20	1	100
6	25	1	100

After heat treatment, the samples were polished and the microstructure was observed by SEM (Apreo C, Waltham, MA, USA) and TEM (JEM-2100, Tokyo, Japan). The chemical composition of the precipitated phase was analyzed by EDS (Apreo C, Waltham, MA, USA). The tensile strength and elongation were measured at room temperature by a universal mechanical testing machine (MTS-E44304, Eden Prairie, MN, USA), and the average value of three samples was taken as the final tensile strength and elongation.

3. Results and Analysis

3.1. Microstructure Analysis

The SEM and mapping scanning result of the precipitated phase of the Al-Cu-Mn-Zr-V alloy after CA treatment is shown in Figure 4. It can be seen that the Cu gathers at the grain boundary while there are small amounts of Mn, Zr, V, and Ti gathering at the grain boundary. All elements are uniformly and diffusely distributed within the grains. The EDS analysis for points 1, 2, and 3 were expressed in Table 3. Point 1 is taken as the θ (Al_2Cu) phase, which is located at the grain boundary; point 2 may be the mixed precipitated phase of Al_3(Ti, Zr, V), which is located within the grain [15]; and point 3 is a dispersed phase distributed within the grain, and it should be $Al_{12}CuMn_2$ according to the atomic ratio and reference [16].

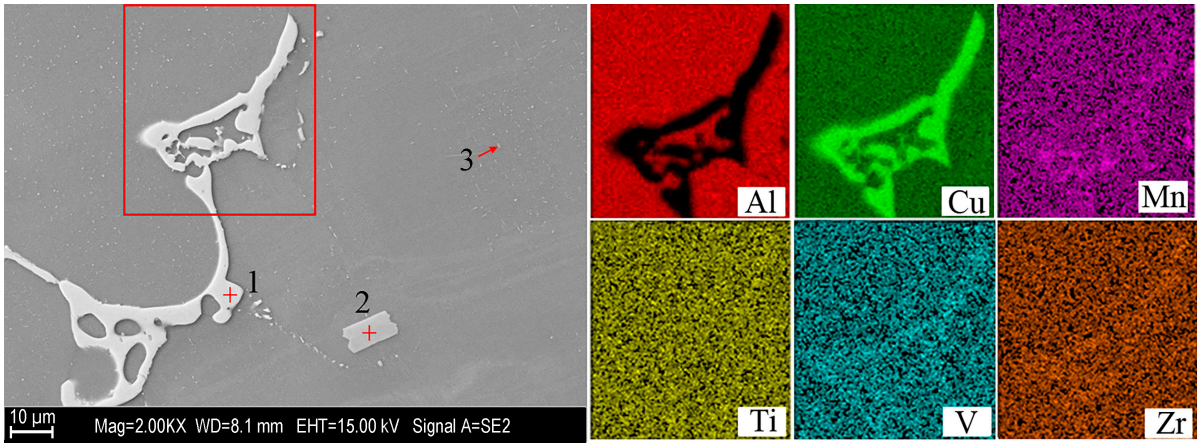


Figure 4. SEM and map scanning of Al-Cu-Mn-Zr-V alloy after conventional ageing treatment.

Table 3. The analysis results of precipitated phase corresponding to Figure 4 (at.%).

Points	Elements					
	Al	Cu	Mn	Zr	V	Ti
1	66.4	33.6	0	0	0	0
2	76.7	0	0	3.2	4.8	15.3
3	89.6	5.7	4.7	0	0	0

The microstructures of the Al-Cu-Mn-Zr-V alloy after CA and AEP treatment are shown in Figure 5. The mechanical properties are closely related to the number and size of precipitates. Figure 5 indicates the electro-pulse has a significant influence on the size and number of θ (Al_2Cu) phase. For the CA treatment, the size of the precipitates is larger, and they are continuously aggregated at the grain boundary. After AEP treatment, the size of the precipitates decreases with the increase of the current density when the current density is less than 15 $A \cdot mm^{-2}$, and the precipitates gradually change from a continuous aggregation distribution to a dispersed distribution at the grain boundary, which improves the tensile strength and fracture toughness of alloys [17,18].

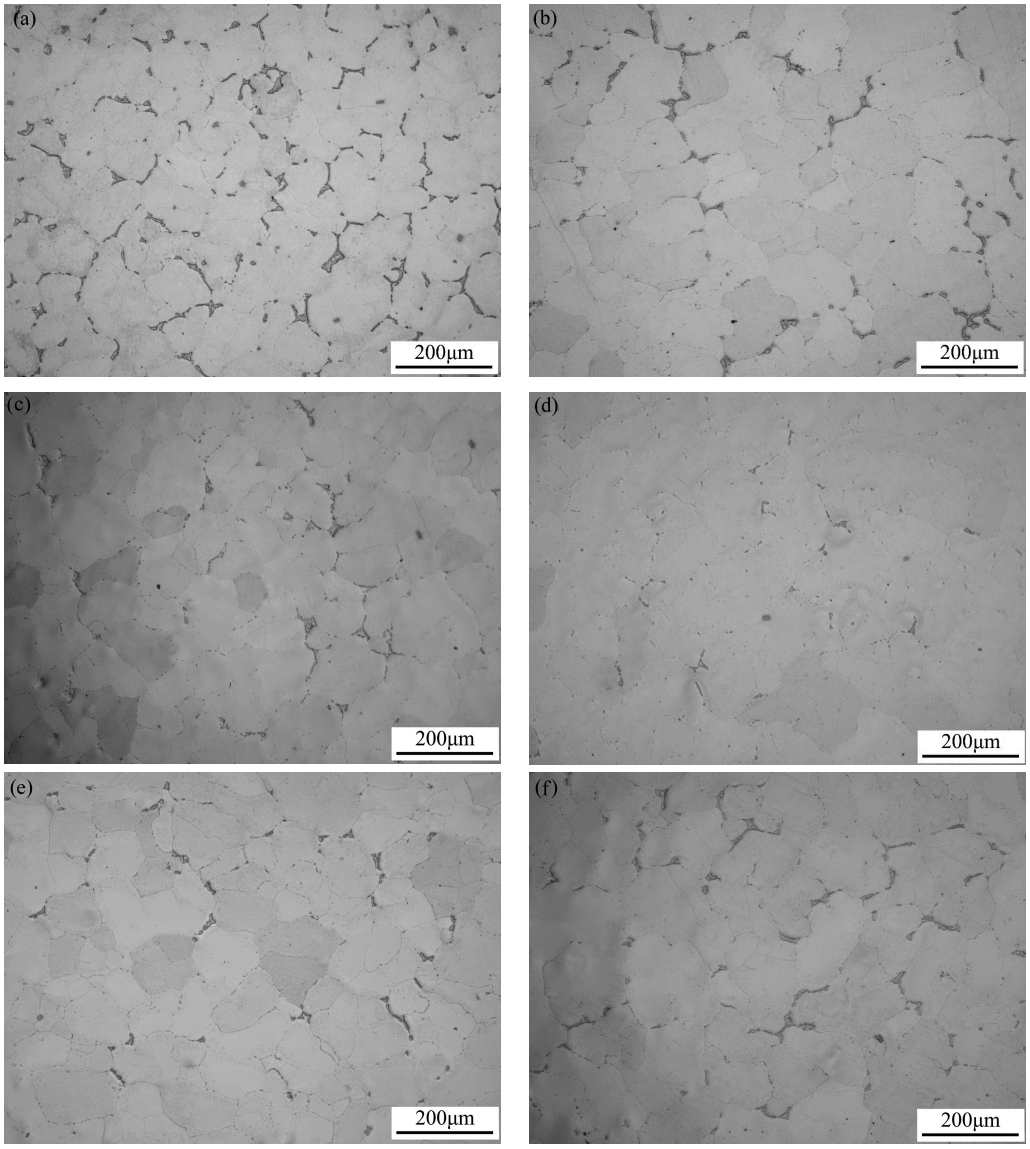


Figure 5. Microstructure of Al-Cu-Mn-Zr-V alloy of conventional ageing (CA) and ageing with electro-pulse (AEP): (**a**) CA, (**b**) 5 A·mm^{-2}, (**c**) 10 A·mm^{-2}, (**d**) 15 A·mm^{-2}, (**e**) 20 A·mm^{-2}, (**f**) 25 A·mm^{-2}.

This can be explained as follows. During the ageing process of samples, the vacancy transition caused by the electro-pulse promotes the formation of GP zone and dissolution of unstable θ′ (Al_2Cu) phase, and the increase of current density further improves the probability of vacancy transition. The Al_3(Ti, Zr, V) core/shell dispersoids are easier to form and significantly refine the θ′ precipitates by acting as preferential nucleation sites during ageing [19]. So, the dissolution degree of the θ′ (Al_2Cu) phase is greater. Both the re-precipitation and dissolution of θ′ (Al_2Cu) will gradually reduce the size and quantity of the precipitates. However, if the current density is greater than 15 A·mm^{-2}, the increase of current density accelerates the formation of a large number of atomic clusters, and the closer atomic clusters will form a larger atomic group [20]. As a consequence, the size and quantity of precipitates increase again, and they are distributed in an aggregated manner. So, the splitting of precipitates on grain boundaries is increased, resulting in the decrease of tensile strength and fracture toughness of alloys.

Figure 6 showed the TEM images, SAED patterns, and HRTEM images of the precipitates along the $[110]_{Al}$ direction after CA treatment and AEP treatment with current density of 15 A·mm^{-2}. Figure 6a,b show that the θ′ (Al_2Cu) phase is uniformly distributed in the α(Al) phase after ageing treatment, and it is needle-like and vertically precipitated

along the two directions of $[010]_{Al}$ and $[001]_{Al}$, which is semi-coherent with the α(Al) phase. The size of the precipitates is 50–100 nm phase in Figure 6a and 30–40 nm in Figure 6b. Compared with CA treatment, the precipitates of AEP treatment become fine, and the quantity is greater and the distribution is uniform. The precipitates in Figure 6b are very concentrated, and some even overlap partially. If the current density further increases, the precipitates will be layered, causing stacking distribution and weakening the strengthening effect of precipitates on the matrix.

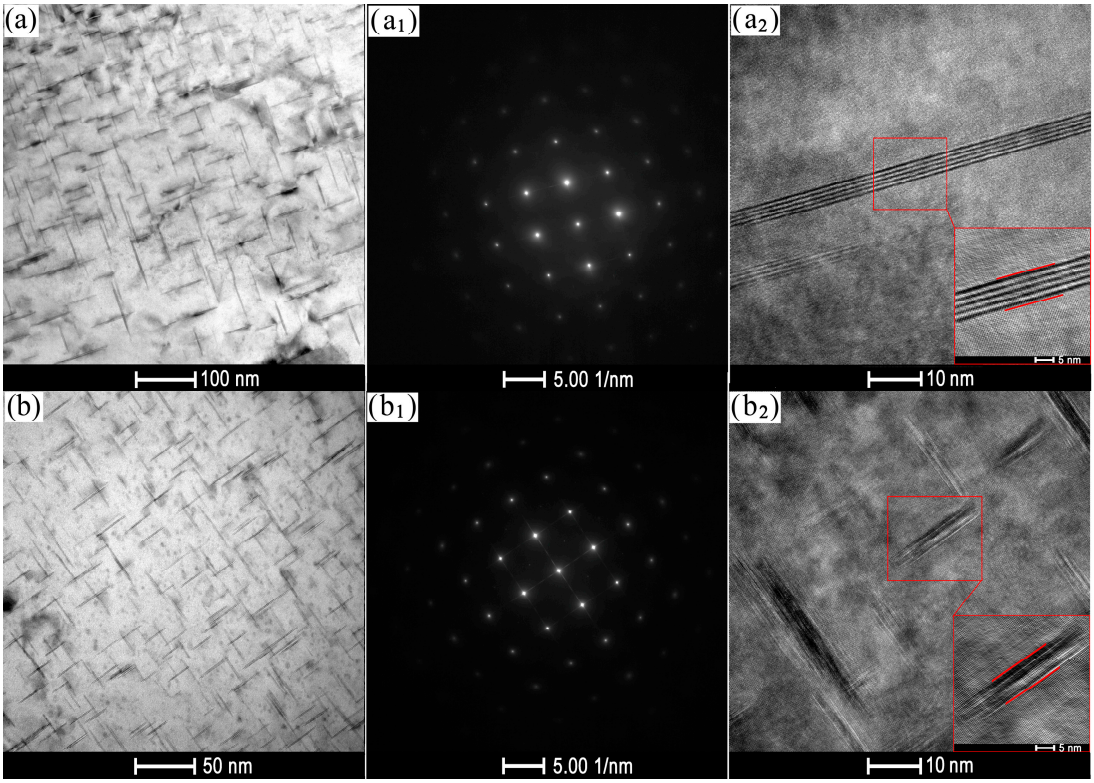


Figure 6. TEM and selected area diffraction spectroscopy of precipitated phase after CA and AEP treatment: (**a**), (**a$_1$**) and (**a$_2$**) CA treatment, (**b**), (**b$_1$**) and (**b$_2$**) AEP treatment with current density of 15 A·mm^{-2}.

In Figure 6(b_1), besides the bright and sharp strong diffraction spots of the precipitates, there are also weak diffraction spots of the α(Al) phase in the center of each of the four adjacent strong diffraction spots. This indicates that the θ′ phase after CA treatment has a more coherent relationship with the α(Al) phase, which results in a greater degree of lattice distortion and better strengthening on the alloys [21]. In addition, there are discontinuous diffraction fringes between every two adjacent diffraction spots in Figure 6(b_1). Some studies have demonstrated that this discontinuous diffraction fringe is caused by the θ″ phase (Al_2Cu), which is a completely coherent friendship with the matrix [22]. Compared with the θ′ phase, the θ″ phase is smaller in size and cannot be observed by an optical microscope. The θ″ phase, which is completely coherent with α(Al), causes greater lattice distortion and thus further improves the strengthening effect.

Figure 6(a_2,b_2) show that the precipitates are θ′ phase for CA treatment while the precipitates are both θ′ and θ″ and the θ′ phase grows on θ″ phase for AEP treatment with current density of 15 A·mm^{-2}. This indicates the electro-pulse not only promotes the nucleation of precipitates, but also inhibits the growth of precipitates and the transformation of θ″ phase to θ′ phase. Fourier transform images of the precipitates illustrate that the θ′ phase widths of two ageing treatments are 16 atomic layers, which proves the electro-pulse only affects the length of precipitates, and it has little effect on the width of precipitates.

3.2. Mechanical Properties Analysis

The mechanical properties of Al-Cu-Mn-Zr-V alloy after ageing treatment are shown in Figure 7, which indicates that the tensile strength and elongation of AEP treatment are higher than those of CA (responding to the current density of 0 A·mm^{-2}). With the increase of current density, the tensile strength and elongation of samples generally increase to the maximum and then decrease. When the current density is 15 A·mm^{-2}, the tensile strength and elongation of samples reach their peak. This is because the electro-pulse promotes nucleation and precipitation, which reduces the size and increases the number of precipitates. In a certain range, with the increase of current density, the size of precipitates decreases and their number increases gradually. Consequently, the mechanical properties of samples increase continuously. When the current density is 15 A·mm^{-2}, the improvement of electro-pulse on the microstructure of the alloy reaches the peak. As the current density continues to increase, the distribution of precipitates gradually shifts to the aggregated stacking, which causes an increase in the splitting effect of precipitates to grain boundaries [23]. At this point, compared with CA treatment, the electro-pulse still plays a positive role in the ageing precipitation of samples. But with the increase of current density, this splitting effect will gradually aggravate, and thus mechanical properties will decrease. The tensile strength and elongation of samples after CA treatment (current density of 0 A·mm^{-2}) are 292.4 MPa and 5.7%. However, after AEP treatment with current density of 15 A·mm^{-2}, they are 443.5 MPa and 8.1%, respectively, which are 51.7% and 42.1% higher than those of CA treatment.

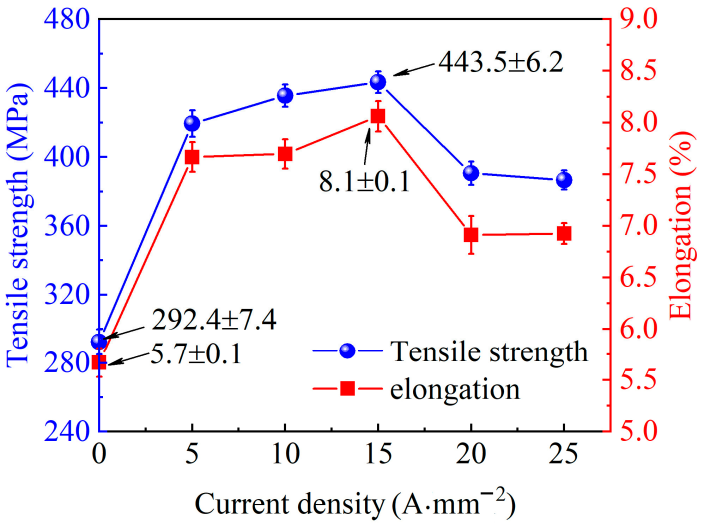


Figure 7. Effect of current density on mechanical properties of Al-Cu-Mn-Zr-V alloy.

4. Mechanism Analysis of Electro-Pulse on Ageing Treatment

4.1. Thermodynamic Analysis

The electro-pulse is an impulsive current that releases the stored energy onto an aluminum alloy sample in a very short time (usually microsecond order of magnitude). Due to the short discharge time, the samples can obtain very large instantaneous power and electrical energy. According to the experiments, when the average current density is within 28.5 A·mm^{-2}, the temperature rise of samples is less than 2 °C, which can be ignored.

According to the theory of current dynamics, when the samples are applied by an alternating current, the current only passes through the surface of samples due to the skin effect. The skin depth of the current in the Al-Cu-Mn-Zr-V alloy samples can be calculated by Equation (1) [24]:

$$\delta = \sqrt{\frac{\rho_s}{\pi f \mu_0 \mu_r}} \quad (1)$$

where ρ_s is the resistivity of the samples with $\rho_s = 59.2 \times 10^{-9}$ Ω·m [25], f is the frequency of the electro-pulse, μ_0 is the vacuum permeability with $\mu_0 = 4\pi \times 10^{-7}$ H·m^{-1}, μ_r is the relative magnetic permeability with $\mu_r = 1$ for Al-Cu-Mn-Zr-V alloy.

The frequency of electro-pulse in this study is 100 Hz, and thus the calculated skin depth is about 12.2 mm. However, the thickness of samples is only 2 mm, so the influence of the skin effect can be ignored.

Due to the different conductivity between the second phase and α-Al matrix, the electro-pulse applied on the samples results in the additional electrical free energy [26], and it significantly alters the original energy state of the system, thereby affecting the evolution process of the microstructure of the alloy. According to the research results of Qin et al. [27], the electrical free energy, ΔG_e, can be written as:

$$\Delta G_e = -\frac{\mu_0}{8\pi}\int_V \int_V \frac{\vec{j}(r')\cdot\vec{j}(r)}{|r-r'|}drdr' \tag{2}$$

where V is the volume of the second phases, r and r' are two different positions in the system, $\vec{j}(r)$ and $\vec{j}(r')$ represent the current density at different positions, and μ_0 is the vacuum magnetic permeability with $\mu_0 = 4\pi \times 10^{-7}$ H·m^{-1}.

The current density can be determined by the conductivity and microstructure of the matrix and second phases. According to the generalized Ohm's law, the current density can be expressed as:

$$\vec{j} = -\sigma\cdot\nabla\varphi \tag{3}$$

where $\vec{j}$ is the current density vector, σ is the conductivity, φ is the potential, and ∇ is the Laplace operator.

At the interface between second phases and the α-Al matrix, the potential meets the following boundary conditions:

$$\sigma_{Al}\frac{\partial\varphi_{Al}}{\vec{n}} = \sigma_{sp}\frac{\partial\varphi_{sp}}{\vec{n}} \tag{4}$$

where σ_{Al} is the conductivity of α-Al matrix, σ_{sp} is the conductivity of the second phases, and $\vec{n}$ is the normal gradient of the interface.

After combining with Equations (2)–(4) and simplifying them, the electrical free energy can be obtained as:

$$\Delta G_e = g\cdot V\cdot\frac{\sigma_{sp}-\sigma_{Al}}{2\sigma_{Al}+\sigma_{sp}}\cdot j^2 \tag{5}$$

where j is the current density of the electro-pulse, and g is a geometric factor and is positive for coarse-grained materials.

The conductivity of α-Al matrix and second phases (assuming all are Al_2Cu) is 3.538×10^7 S·m^{-1} and 1.053×10^7 S·m^{-1}, respectively [28,29]. Due to $\sigma_{Al} > \sigma_{sp}$, therefore $\Delta G_e < 0$. Therefore, the additional electrical free energy, ΔG_e, will cause the decrease of free energy in the system, and the reaction always proceeds in the direction of decreasing free energy, thereby creating thermodynamic conditions for accelerating the precipitation of second phases in Al-Cu-Mn-Zr-V alloy.

Equation (5) indicates that the absolute value of electrical free energy, ΔG_e, is proportional to the square of current density j. As the current density j increases, the electrical free energy becomes more negative, the decrease of free energy ΔG in the system is greater, and accordingly the possibility of precipitating second phases goes higher.

According to classical thermodynamic theory, the precipitation of second phases must provide sufficient energy to overcome energy barriers. Before applying an electro-pulse,

the critical temperature, T_h, where the second phase precipitates from the matrix can be determined by:

$$T_h = \frac{\Delta H}{\Delta S} \tag{6}$$

where ΔH and ΔS are the enthalpy change and entropy change of the system, respectively, $\Delta H > 0$ and $\Delta S > 0$.

After the electro-pulse was applied, the critical temperature, T_{ep}, for the precipitation of the second phases is given by:

$$T_{ep} = \frac{\Delta H + \Delta G_e}{\Delta S} \tag{7}$$

Due to $\Delta G_e < 0$, obviously $T_{ep} < T_h$, indicating that when the electro-pulse was applied, the electrical free energy ΔG_e reduces the thermodynamic energy barrier for the precipitation of second phases from an Al-Cu-Mn-Zr-V alloy, that is, the precipitation temperature of second phases will be decreased. This macroscopically expresses that the alloy can undergo a shorter ageing time or a lower temperature under the electro-pulse.

4.2. Kinetic Analysis

Ageing precipitation essentially belongs to the solid-state phase transition controlled by solute atom diffusion, and the diffusion of displaced solute atoms in Al-Cu alloy is closely related to the vacancy migration [30]. Due to the fact that the nucleation rate in Al-Cu-Mn-Zr-V alloy is significantly lower than the grain growth rate, the ageing process is mainly determined by the nucleation rate. The following are dynamic analyses of the diffusion coefficient, nucleation rate, and grain growth in Al-Cu-Mn-Zr-V alloy under the action of thermal and electro-pulse fields.

Under the electro-pulse, high-speed electrons collide with metal atoms, and the metal atoms will be subjected to the electronic thrust. Assuming that a metal atom jumps from one vacancy to an adjacent one, the work, ΔW, performed by the electron wind force can be expressed as [31,32]:

$$\Delta W = |e| \cdot Z^* \cdot \rho \cdot j \cdot b \tag{8}$$

where $|e|$ is the electron charge, Z^* is the effective valence, and ρ is the electrical resistivity of metal atoms, and b is the Burgers vector modulus of the Cu atom.

Due to the inelastic collision between electrons and atoms, some of their kinetic energy is converted into internal energy, resulting in Joule heat. Therefore, the kinetic energy ΔW_e obtained by metal atoms under the electro-pulse field can be expressed as:

$$\Delta W_e = \Delta W \cdot (1 - \eta_v) \cdot N_A \tag{9}$$

where η_v is the Joule heat fraction, which represents the percentage of work done by the electronic wind force being converted into Joule heat; N_A is the Avogadro constant.

Due to the FCC structure of Al-Cu-Mn-Zr-V alloy, the probability of transition from the centroid to the vertex is $\omega = 1/12$, and the coordination number is $C_N = 12$. Therefore, based on present research results [33], the diffusion coefficient of the Al-Cu-Mn-Zr-V alloy can be written as:

$$D_v = a^2 \cdot \nu \cdot \exp\left(-\frac{Q}{RT}\right) \tag{10}$$

where D_v is the volume diffusion coefficient of solute atoms, a is the transition distance of an atom, ν is the vibrational frequency of the atom at its equilibrium position, R is the molar gas constant, T is the ageing temperature, and Q is the activation energy.

During the ageing treatment, the copper atoms diffuse according to the vacancy mechanism, which requires to overcome the Gibbs free energies of vacancy formation ΔG_f and vacancy migration ΔG_m; therefore, the activation energy Q can be represented as:

$$\begin{aligned} Q &= \Delta G_f + \Delta G_m - \Delta W_e \\ &= (\Delta H_f - T\Delta S_f) + (\Delta H_m - T\Delta S_m) - \Delta W_e \end{aligned} \quad (11)$$

According to Equations (8)–(11), one can conclude that:

$$\begin{aligned} D_v &= a^2 \cdot \nu \cdot \exp\left(\frac{\Delta S_f + \Delta S_m}{R}\right) \cdot \exp\left(-\frac{\Delta H_f + \Delta H_m - (1-\eta_v)\cdot|e|\cdot Z^* \cdot \rho \cdot j \cdot b \cdot N_A}{RT}\right) \\ &= D_{v0} \cdot \exp\left(-\frac{\Delta H_f + \Delta H_m}{RT} + \frac{(1-\eta_v)\cdot|e|\cdot Z^* \cdot \rho \cdot j \cdot b \cdot N_A}{RT}\right) \end{aligned} \quad (12)$$

where D_{v0} is the pre-diffusion constant, ΔH_f and ΔH_m represent the enthalpy changes caused by vacancy formation and migration, respectively, and ΔS_f and ΔS_m represent the entropy changes caused by vacancy formation and migration, respectively.

Equation (12) expresses that the electro-pulse reduces the diffusion activation energy of atoms, thereby promoting atomic diffusion.

The diffusion behavior of a Cu atom under electro-pulse can be studied by solving Equation (12). The adopted parameters are as follows. $D_{v0} = 8.4 \times 10^{-6}$ $m^2 \cdot s^{-1}$ [34], $\Delta H_f + \Delta H_m = 1.36 \times 10^5$ $J \cdot mol^{-1}$ [35], $\eta_v = 0.77$ [36], $|e| = 1.6 \times 10^{-19}$ C, $Z^* = 13.201$ [37], $b = 0.2556$ [38], $\rho = 1.86 \times 10^{-8}$ $\Omega \cdot m$ [39], $R = 8.314$ $J \cdot (mol \cdot K)^{-1}$, and $N_A = 6.02 \times 10^{23}$ mol^{-1}. The calculated diffusion coefficients at 453 K, 463 K, and 473 K are shown in Figure 8.

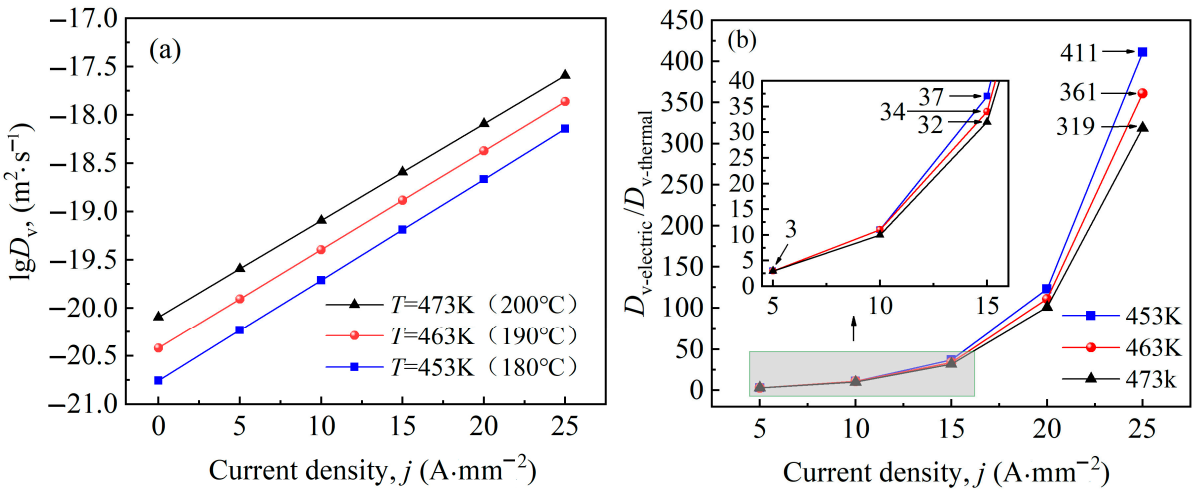


Figure 8. The calculation results of diffusion coefficients of Cu atoms at 453 K, 463 K, and 473 K: (**a**) relationship between logarithmic diffusion coefficients and current density, (**b**) relationship between diffusion coefficient ratio of electro-pulse to thermal fields and current density.

Figure 8a shows that the logarithmic diffusion coefficients gradually increase with the increase of the current density, but at the same temperature, the diffusion coefficients have a significant difference between the electro-pulse field and thermal field. At the ageing temperature of 463 K, the diffusion coefficient for the thermal field (corresponding to a current density $j = 0$ $A \cdot mm^{-2}$) is 3.81×10^{-21} $m^2 \cdot s^{-1}$ while it is 1.30×10^{-19} $m^2 \cdot s^{-1}$ for the electro-pulse field with $j = 15$ $A \cdot mm^{-2}$, which is approximately 34 times of the thermal field. If the current density further increases, when $j = 20$ $A \cdot mm^{-2}$, the diffusion coefficient of Cu atoms (4.23×10^{-19} $m^2 \cdot s^{-1}$) is increased by approximately 110 times. When $j = 25$ $A \cdot mm^{-2}$, the diffusion coefficient (1.37×10^{-18} $m^2 \cdot s^{-1}$) is increased by approximately 360 times.

Figure 8b expresses that the diffusion coefficient ratio of electro-pulse field to thermal field increases exponentially with the increase of current density. The ratio of $D_{v\text{-electric}}$

to $D_{\text{v-thermal}}$ increases from 3 at j = 5 A·mm^{-2} to 32 at j = 15 A·mm^{-2} and then increases to 319 at j = 25 A·mm^{-2}. At lower ageing temperature, the ratio of $D_{\text{v-electric}}$ to $D_{\text{v-thermal}}$ increases faster with current density, indicating that the electro-pulse can play a greater role at lower ageing temperature, and significantly promoting the diffusion rate of Cu atoms and accelerating the ageing precipitation. In addition, for the low current density with j = 5 A·mm^{-2}, the ratio of $D_{\text{v-electric}}$ to $D_{\text{v-thermal}}$ at three temperatures is about 3, that is, the electro-pulse and thermal fields have the same contribution to the diffusion coefficient. However, when the current density is increased to 10 A·mm^{-2} or above, the contribution of electro-pulse fields to the diffusion coefficient is much larger than that of thermal field. At this time, the low temperature and high current density can be used to be ageing treatment for Al-Cu-Mn-Zr-V alloy.

Since grain boundaries only account for a small portion of the sample cross-section, the contribution of grain boundaries to the atomic diffusion flux depends on the relative cross-sectional area through which the atoms pass. The effective diffusion coefficient of grain boundaries can be expressed as:

$$D_{\text{b}} = \frac{\delta}{d} \cdot D_{\text{b0}} \cdot \exp\left(-\frac{\Delta H_{\text{bf}} + \Delta H_{\text{bm}} - (1-\eta_{\text{b}}) \cdot |e| \cdot Z^* \cdot \rho \cdot j \cdot b \cdot N_{\text{A}}}{RT}\right) \tag{13}$$

where D_{b} is the diffusion coefficient of grain boundaries, δ is the effective width of grain boundaries with $\delta \approx 0.5$ nm for Al-Cu alloy [40], d is the average grain size, which can be measured by ImageJ2 software with d = 157 μm, D_{b0} is the pre-diffusion constant at grain boundaries with $D_{\text{b0}} = 2 \times 10^{-4}$ m^2·s^{-1} [41], $\Delta H_{\text{bf}} + \Delta H_{\text{bm}}$ is the activation energy of grain boundary diffusion with $\Delta H_{\text{bf}} + \Delta H_{\text{bm}} = 8.97 \times 10^4$ J·mol^{-1} [42], and $\eta_{\text{b}} = 0.89$ [43].

For the ageing temperature of 463 K, the diffusion coefficients of Cu atoms at grain boundaries under different current density are shown in Figure 9.

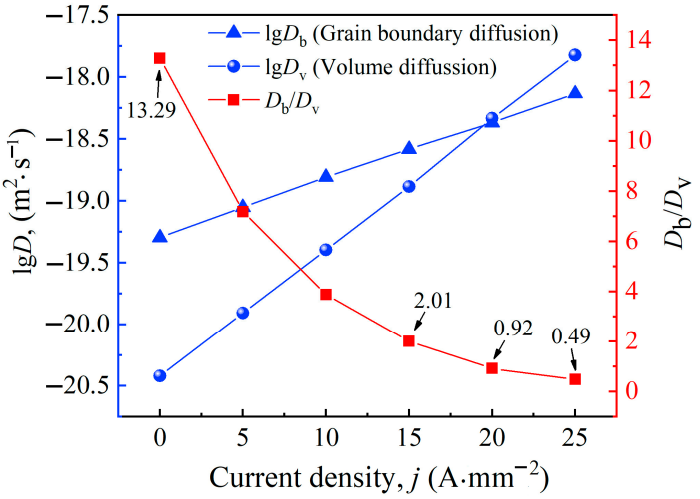


Figure 9. Variation of the calculated boundary and volume diffusion coefficients at 463 K as well as their ratio with current density.

One can see that the boundary diffusion coefficients are higher than the volume diffusion coefficients due to the low activation energy of grain boundary diffusion when the current density is low, and there is a maximum difference of one order of magnitude between them for the current density of 0 A·mm^{-2}. As the current density increases, the effect of the electro-pulse becomes more significant, the vacancy concentration within grains gradually increases, the diffusion rate of atoms rapidly increases, and accordingly the difference of diffusion coefficients gradually decreases. When the current density is 15 A·mm^{-2}, the ratio of boundary diffusion coefficient to volume diffusion coefficient decreases from 13.29 to 2.01, with 2.62×10^{-19} m^2·s^{-1} and 1.32×10^{-19} m^2·s^{-1}, respectively. When the current density is 20 A·mm^{-2}, the boundary diffusion coefficient (4.31×10^{-19} m^2·s^{-1}) is slightly

less than the volume diffusion coefficient (4.62×10^{-19} $m^2 \cdot s^{-1}$), and the ratio is close to 1. When the current density is increased to 25 $A \cdot mm^{-2}$, the volume diffusion coefficient continues to increase, and the grain boundary diffusion coefficient (7.36×10^{-19} $m^2 \cdot s^{-1}$) is approximately half of the volume diffusion coefficient (1.51×10^{-18} $m^2 \cdot s^{-1}$).

Therefore, the electro-pulse during the ageing can effectively enhance the diffusion coefficient and accelerate the precipitation of second phases. However, as the current density increases, the increment of boundary diffusion coefficient is smaller than that of volume diffusion coefficient. As a consequence, the precipitates at grain boundaries gradually decrease, resulting in an increase of the mechanical properties of the alloy. When the current density increases to a certain extent (15 $A \cdot mm^{-2}$ in this study), the boundary diffusion coefficient is smaller than the volume diffusion coefficient, and the second phases at the grain boundaries begin to grow again, causing a decrease of the mechanical properties of the alloy.

According to the classical nucleation theory, nucleation is the formation process of stable cores of precipitated phases from supersaturated solid solutions due to local component fluctuations [44]. In the early stage of ageing treatment, the nucleation driving force is large and the second phase is easy to precipitate. For an Al-Cu alloy, the second phases can precipitate by the heterogeneous nucleation adhering to T phase [45], but due to the small number, most of the second phases will precipitate in a homogeneous nucleation manner. The nucleation rate can be expressed as [46]:

$$\frac{dN}{dt} = N_0 Z \beta^* \exp\left(-\frac{\Delta G^*}{k_b T}\right) \exp\left(-\frac{\tau}{t}\right) \tag{14}$$

where N is the number density of precipitates, N_0 is the number of nucleation site per unit volume in the solid solution, Z is the Zeldovich factor with $Z \approx 0.05$, ΔG^* is the critical nucleation barrier, k_b is the Boltzmann constant, T is the ageing temperature, t is the ageing time, τ is the incubation time for nucleation with $\tau = (2\beta^* Z)^{-1}$ [47], and β^* is the condensation rate of solute atoms in a cluster of critical radius r^*, and for an Al-Cu-Mn-Zr-V alloy β^* can be represented as [48]:

$$\beta^* = 4\pi (r^*)^2 C_0 D_v a_0^{-4} \tag{15}$$

where C_0 is the matrix mean solute atom fraction, a_0 is the lattice parameter of precipitates.

By substituting Equation (15) into (14), the nucleation rate of the second phases during the ageing process can be expressed as:

$$\frac{dN}{dt} = k_1 \cdot D_v \exp\left(-\frac{\Delta G^*}{k_b T}\right) \exp\left(-\frac{\tau}{t}\right) \tag{16}$$

where $k_1 = N_0 Z 4\pi (r^*)^2 C_0 D_v a_0^{-4}$, and for a fixed component Al-Cu-Mn-Zr-V alloy, k_1 can be regarded as a constant. Therefore, it can be clearly seen from Equation (16) that when the aluminum alloy with a specific composition is aged at a given temperature, the key parameters for predicting the continuous nucleation rate with ageing time are the diffusion coefficient D_v and nucleation activation energy ΔG^*.

Before electro-pulse was applied, whether the second phases can precipitate from the supersaturated solid solution mainly depends on the chemical free energy ΔG_c, interface free energy ΔG_i, and strain free energy ΔG_s, and they can be represented as [49]:

$$\begin{cases} \Delta G_c = -\left(\pi r_{sp}^2 l_{sp} - \frac{2}{3}\pi r_{sp}^3\right)\Delta g_c \\ \Delta G_i = 2\pi r_{sp} l_{sp} \gamma \\ \Delta G_s = \left(\pi r_{sp}^2 l_{sp} - \frac{2}{3}\pi r_{sp}^3\right)\Delta g_s \end{cases} \tag{17}$$

where r_{sp} and l_{sp} are the length and radius of the precipitated second phase, respectively, and Δg_c and Δg_s correspond to the chemical free energy and strain energy per unit volume, respectively.

The changes of Gibbs free energy with the radius of precipitate phase under different fields are shown in Figure 10a.

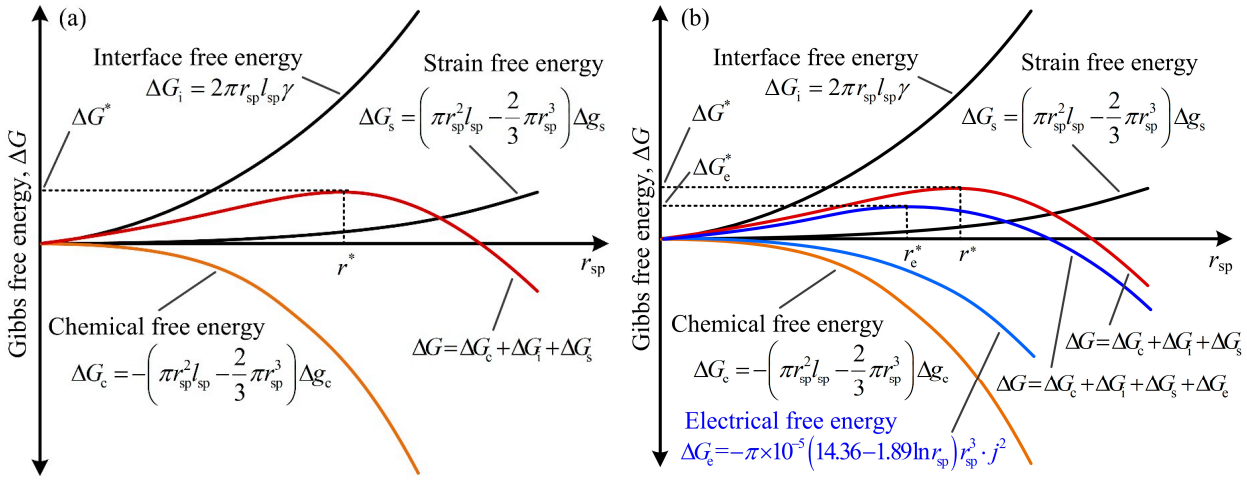


Figure 10. Change of Gibbs free energy of nucleation process with the size of precipitate phase: (**a**) before electro-pulse was applied, (**b**) after electro-pulse was applied.

After the electro-pulse was applied, owing to the contribution of electrical free energy, the critical nucleation activation energy is changed to $\Delta G_e^* = \max\{\Delta G_c + \Delta G_i + \Delta G_s + \Delta G_e\}$, and the nucleation rate is rewritten as:

$$\begin{aligned} \frac{dN}{dt} &= k_1 \cdot D_v \exp\left(-\frac{\max\{\Delta G_c + \Delta G_i + \Delta G_s + \Delta G_e\}}{k_b(T + T_e)}\right) \exp\left(-\frac{\tau}{t}\right) \\ &\approx k_1 \cdot D_v \exp\left(-\frac{\max\{\Delta G_c + \Delta G_i + \Delta G_s + \Delta G_e\}}{k_b T}\right) \exp\left(-\frac{\tau}{t}\right) \end{aligned} \quad (18)$$

where T_e is the temperature rise of the sample caused by the electro-pulse, and it can be ignored due to $T_e < 2\ ^\circ C$.

Assuming that all second phases are Al_2Cu, according to the results of Qin et al. [50], the geometric factor, g, coefficient in Equation (5) can be expressed as:

$$g = \left[\frac{3}{2}\ln\left(\frac{\delta_0}{r_{sp}}\right) - \frac{65}{48} - \frac{5}{48} \cdot \frac{\sigma_{sp} - \sigma_{Al}}{2\sigma_{Al} + \sigma_{sp}}\right] \mu_0 \delta_0^2 \quad (19)$$

where $\mu_0 = 4\pi \times 10^{-7}$ H·m^{-1}, $\sigma_{Al} = 3.538 \times 10^7$ S·m^{-1}, $\sigma_{sp} = 1.053 \times 10^7$ S·m^{-1}, and δ_0 is the linearity of the sample with $\delta_0 = 5$ mm in this experiment.

By substituting Equation (19) and $V = \frac{4}{3}\pi r_{sp}^3$ into Equation (5), the electrical free energy ΔG_e can be simplified as:

$$\Delta G_e = -\pi \times 10^{-5}\left(14.36 - 1.89 \ln r_{sp}\right) r_{sp}^3 \cdot j^2 \quad (20)$$

where the units of r_{sp} and j are μm and A·mm^{-2}, respectively.

It can be concluded that $\left(14.36 - 1.89 \ln r_{sp}\right) > 0$ due to the small radius r_{sp} of second phases, and thus $\Delta G_e < 0$. Therefore, the electrical free energy ΔG_e is the driving force for phase transition, resulting in the decrease of critical nucleation activation energy and accordingly promoting the nucleation of second phases. After the electro-pulse was applied, the change of Gibbs free energy of nucleation process with the size of precipitate phase is shown in Figure 10b.

Figure 10a indicates that when $r_{sp} \leq r^*$, the Gibbs free energy increases with the increase of r_{sp}. When $r_{sp} > r^*$, the Gibbs free energy decreases as the r_{sp} increases. Thus, only

nuclei with a size greater than r^* can exist stably. After the electro-pulse is applied, as shown in Figure 10b, the critical nucleation activation energy ΔG^* of the system significantly decreases to ΔG_e^*, and the nucleation rate of second phases increases exponentially according to Equation (18). Therefore, the electro-pulse can make the second phases nucleate at lower Gibbs free energy, and the second phases become finer.

Equation (20) indicates that as the current density increases, the electrical free energy ΔG_e decreases by square, and the decrements of ΔG^* and r^* are greater. However, small-sized precipitates are less stable than large ones. At a constant volume fraction, small-sized precipitates will then shrink until complete dissolution to the benefit of large ones, which will preferentially grow [51], leading to a continuous increase in the particle average size. This is the so-called coarsening mechanism made by Lifchitz, Slyosov, and Wagner [52,53]. The LSW theory for coarsening kinetics can be expressed as [54]:

$$\bar{r}^3 - \bar{r}_0^3 = K \cdot t \tag{21}$$

where $\bar{r}$ and $\bar{r}_0$ are the average radii of the precipitates at time t and at the onset of the coarsening process, respectively, and K is the growth rate coefficient.

The growth rate coefficient, K_h, contributed by the thermal field can be given by [55]:

$$K_h = \frac{8\gamma D_v V_m C_\infty}{9RT} \tag{22}$$

where V_m is the average molar volume of the precipitates and C_∞ is the equilibrium concentration of the solute atoms in the matrix at the temperature T.

Under the electro-pulse, in addition to the coarsening behavior predicted by the classical LSW theory, two other factors, the electromigration caused by drift electrons and the diffusion coefficient affected by the interaction between drift electrons and quenched vacancies, are also considered to contribute to the coarsening of precipitates. Conrad concluded that currents with a density of 10 $A \cdot mm^{-2}$ or above can accelerate the solid-state phase transition of alloys by promoting atomic diffusion [56]. Therefore, electromigration may play a crucial role in the coarsening of precipitates. According to the Nernst–Einstein Equation, the drift flux of solute atoms caused by electromigration can be expressed as [57]:

$$J_e = \frac{N \cdot N_A D_v Z^* |e| \rho j}{RT} \tag{23}$$

where J_e is the drift flux of solute atoms, and N is the atomic density of solute atoms.

Assuming that the contribution ratio of electromigration to the coarsening of precipitates is α, another growth rate coefficient, K_e, related to electromigration can be determined as [58]:

$$K_e = \alpha \frac{n V_e D_v Z^* |e| \rho j}{RT} \tag{24}$$

where n is the molar number of the solute atoms per unit volume, V_e is the molar volume increment of precipitates formed by absorbing drift atoms caused by electromigration.

So, based on Equations (22) and (24), and combined with Equation (12), the growth rate coefficient, K, of precipitates corresponding to the electro-pulse process is written as:

$$\begin{aligned} K = K_h + K_e &= \left(\frac{8\gamma V_m C_\infty}{9RT} + \alpha \frac{n V_e Z^* |e| \rho j}{RT} \right) D_v \\ &= \left(\frac{8\gamma V_m C_\infty}{9RT} + \alpha \frac{n V_e Z^* |e| \rho j}{RT} \right) \cdot D_h \exp\left(\frac{(1-\eta_v)|e| Z^* \rho j b N_A}{RT} \right) \end{aligned} \tag{25}$$

where D_h is the diffusion coefficient only under the action of the thermal field with $D_h = a^2 \nu \exp\left(\frac{\Delta S_f + \Delta S_m}{R}\right) \exp\left(-\frac{\Delta H_f + \Delta H_m}{RT}\right)$.

Due to $\frac{(1-\eta_v) \cdot |e| \cdot Z^* \cdot \rho \cdot j \cdot b \cdot N_A}{RT} > 0$ and $\exp\left(\frac{(1-\eta_v)|e| Z^* \rho j b N_A}{RT}\right) >> 1$, the growth coefficient of precipitates aged with AEP is much higher than that of precipitates only aged by CA.

According to Equation (21), the electro-pulse can accelerate the coarsening of precipitates, and the higher the current density, the more severe the coarsening of precipitates.

Therefore, although the electro-pulse can make the second phases nucleate and precipitate at a lower Gibbs free energy and the radius of the precipitates is smaller than before, it also accelerates the growth and coarsening of the precipitates. There is an appropriate current density that allows the second phases to rapidly nucleate while growing into smaller particles. In this study, the appropriate current density is 15 A·mm^{-2}. This also explains why the microstructure in Figure 5 first becomes fine and then coarse as the current density increases.

5. Conclusions

(1) Electro-pulse has a significant influence on the size and quantity of precipitates in the aged Al-Cu-Mn-Zr-V alloy. As the current density increases, the size and quantity of precipitates continue to decrease, gradually transforming from continuous aggregated distribution at grain boundaries to dispersed distribution. But when the current density exceeds 15 A·mm^{-2}, the size and quantity of precipitates begin to increase again and aggregate at grain boundaries.

(2) Electro-pulse significantly improves the mechanical properties of Al-Cu-Mn-Zr-V alloy. With the increase of current density, the mechanical properties increase, and when the current density is 15 A·mm^{-2}, the mechanical properties reach a peak, with a tensile strength of 443.5 MPa and an elongation of 8.1%, which are 51.7% and 42.1% higher than conventional ageing treatment, respectively.

(3) Electro-pulse provides thermodynamic and kinetic conditions for ageing precipitation of the second phases in the form of additional electrical free energy. The negative electrical free energy is the driving force for phase transformation. The higher the current density, the better the thermodynamic basis for the alloy to precipitate the second phases at a lower ageing temperature.

(4) Electro-pulse enhances the diffusion coefficient, nucleation rate, and grain growth rate of Al-Cu-Mn-Zr-V alloy during ageing treatment. At the temperature of 463 K, the diffusion coefficient at 15 A·mm^{-2} is approximately 34 times that of thermal field. Electro-pulse improves the nucleation rate by increasing the diffusion coefficient and reducing the critical nucleation activation energy, as well as reduces the critical nucleation radius of the second phases. However, it also accelerates the growth and coarsening of grains, making the second phases coarser than before. There is an appropriate current density of electro-pulse, which is 15 A·mm^{-2} for this study, that allows the second phases to more rapidly nucleate while growing into smaller particles.

Author Contributions: Conceptualization, D.S. and G.G.; Methodology, D.S. and W.Y.; Investigation, D.S., G.G. and K.K.; Visualization, D.S. and W.Y.; Writing—review and editing, D.S.; Supervision, D.S.; Writing—original draft, G.G. and K.K.; Data curation, K.K. and W.Y.; Formal analysis, D.S. and G.G. All authors have read and agreed to the published version of the manuscript.

Funding: The authors were sponsored by the Key Technology Research and Development Program of Heilongjiang Province (GA21A103).

Data Availability Statement: The raw data supporting the conclusions of this article will be made available by the authors on request.

Conflicts of Interest: The authors declare no conflicts of interest.

References

1. Luo, A.A.; Sachdev, A.K.; Apelian, D. Alloy development and process innovations for light metals casting. *J. Mater. Process. Technol.* **2022**, *360*, 117606. [CrossRef]
2. Su, R.M.; Jia, Y.X.; Xiao, J.; Li, G.L.; Qu, Y.D.; Li, R.D. Effect of secondary aging on microstructure and properties of cast Al-Cu-Mg alloy. *China Foundry* **2023**, *20*, 71–77. [CrossRef]

3. Sun, T.; Geng, J.; Bian, Z.; Wu, Y.; Wang, M.; Chen, D.; Ma, N.; Wang, H. Enhanced thermal stability and mechanical properties of high-temperature resistant Al-Cu alloy with Zr and Mn micro-alloying. *Trans. Nonferrous Met. Soc. China* **2022**, *32*, 64–78. [CrossRef]
4. Koshmin, A.; Cherkasov, S.; Fortuna, A.; Gamin, Y.; Churyumov, A. Optimization of flat-rolling parameters for thermally stable alloy of Al-Cu-Mn System with micro additions of Si and Zr. *Metals* **2023**, *13*, 2019. [CrossRef]
5. Li, D.; Liu, K.; Rakhmonov, J.; Chen, X.G. Enhanced thermal stability of precipitates and elevated-temperature properties via microalloying with transition metals (Zr, V and Sc) in Al-Cu 224 cast alloys. *Mater. Sci. Eng. A* **2021**, *827*, 142090. [CrossRef]
6. Cai, Z.; Liu, H.; Wang, R.; Peng, C.; Feng, Y.; Wang, X. Microstructure and mechanical properties of the extruded Al-Cu-Mn-Sc-Zr alloy during single-stage and two-stage aging. *J. Mater. Eng. Perform.* **2023**, *32*, 185–198. [CrossRef]
7. Michi, R.A.; Sisco, K.; Bahl, S.; Allard, L.F.; Wagner, K.B.; Poplawsky, J.D.; Leonard, D.N.; Dehoff, R.R.; Plotkowski, A.; Shyam, A. Microstructural evolution and strengthening mechanisms in a heat-treated additively manufactured Al-Cu-Mn-Zr alloy. *Mater. Sci. Eng. A* **2022**, *840*, 142928. [CrossRef]
8. Yakovtseva, O.A.; Mochugovskiy, A.G.; Prosviryakov, A.S.; Bazlov, A.I.; Emelina, N.B.; Mikhaylovskaya, A.V. The microstructure and properties of Al-Mn-Cu-Zr alloy after high-energy ball milling and hot-press sintering. *Metals* **2024**, *14*, 310. [CrossRef]
9. Wang, J.; Qi, J.; Zhao, Z.; Guo, H.; Zhao, T. Effects of electric pulse modification on liquid structure of Al-5%Cu alloy. *Trans. Nonferrous Met. Soc. China* **2013**, *23*, 2792–2796. [CrossRef]
10. Li, N.; Zhang, L.; Zhang, R.; Yin, P.; Xing, H.; Wu, H. Research on grain refinement in hypoeutectic Al-Si alloy during solidification under an alternating electric current pulse. *Metals* **2019**, *9*, 571. [CrossRef]
11. Liu, Y.Z.; Huang, M.H.; Ma, Z.Y.; Zhan, L.H. Influence of the low-density pulse current on the ageing behavior of AA2219 aluminum alloy. *J. Alloys Compd.* **2016**, *673*, 358–363. [CrossRef]
12. Chen, Z.; Li, B.; Huang, Q.; Zhang, L.; Liu, J. The effect of the electric pulse treatment on the microstructure and mechanical performance of the Al-Zn alloy. *Mater. Sci. Eng. A* **2020**, *796*, 140016. [CrossRef]
13. Bian, T.J.; Li, H.; Lei, C.; Wu, C.H.; Zhang, L.W. Microstructures and properties evolution of Al-Zn-Mg-Cu alloy under electrical pulse assisted creep aging. *Adv. Manuf.* **2022**, *10*, 596–609. [CrossRef]
14. Kang, K.J.; Li, D.Y.; Shi, D.Q.; Gao, G.L.; Xu, Z.Y.; Wang, L. Evolution of microstructure and mechanical properties in Al-Zn-Mg-Cu alloy by electric pulse aging treatment. *Trans. Indian Inst. Met.* **2021**, *74*, 2835–2842. [CrossRef]
15. Jia, Z.H.; Couzinie, J.P.; Cherdoudi, N. Precipitation behaviour of Al_3Zr precipitate in Al-Cu-Zr and Al-Cu-Zr-Ti-V alloys. *Trans. Nonferrous Met. Soc.* **2012**, *22*, 1860–1865. [CrossRef]
16. Meng, F.S.; Wang, Z.; Zhao, Y.L.; Zhang, D.; Zhang, W. Microstructures and properties evolution of Al-Cu-Mn alloy with addition of Vanadium. *Metals* **2016**, *7*, 10. [CrossRef]
17. Askari-paykani, M.; Meratian, M.; Shayan, M.; Raeissi, K. Effects of heat treatment parameters on microstructural changes and corrosion behavior of Al 7075 alclad alloy. *Anti-Corros. Methods Mater.* **2012**, *59*, 231–238. [CrossRef]
18. Kumar, N.; Sharma, A.; Dwivedi, D.; Ahn, B.; Manoj, M.K. Influence of various heat treatment procedures on the corrosion behavior of Al-Zn-Mg-Cu alloys. *Mater. Res. Express* **2019**, *6*, 126554. [CrossRef]
19. Jiang, L.; Rouxel, B.; Langan, T.; Dorin, T. Coupled segregation mechanisms of Sc, Zr and Mn at θ′ interfaces enhances the strength and thermal stability of Al-Cu alloys. *Acta Mater.* **2021**, *206*, 116634. [CrossRef]
20. Buyukdogan, S.; Gunduz, S.; Turkmen, M. Influence of aging treatment on microstructure, mechanical properties and adhesive wear behaviour of 6063 aluminium alloy. *Ind. Lubr. Tribol.* **2014**, *66*, 520–524. [CrossRef]
21. Gao, L.; Li, K.; Ni, S. The growth mechanisms of θ′ precipitate phase in an Al-Cu alloy during aging treatment. *J. Mater. Sci. Technol.* **2021**, *61*, 25–32. [CrossRef]
22. Takeda, M.; Komatsu, A.; Ohta, M.; Shirai, T.; Endo, T. The influence of Mn on precipitation behavior in Al-Cu. *Scr. Mater.* **1998**, *39*, 1295–1300. [CrossRef]
23. Duan, S.W.; Matsuda, K.; Wang, T. Microstructures and mechanical properties of a cast Al-Cu-Li alloy during heat treatment procedure. *Rare Met.* **2021**, *40*, 1897–1906. [CrossRef]
24. Psyk, V.; Risch, D.; Kinsey, B.L.; Tekkaya, A.E.; Kleiner, M. Electromagnetic forming—A review. *J. Mater. Process. Technol.* **2011**, *211*, 787–829. [CrossRef]
25. Aksoz, S.; Ocak, Y.; Marasli, N.; Cadirli, E.; Kaya, H.; Boyuk, U. Dependency of the thermal and electrical conductivity on the temperature and composition of cu in the Al based Al-Cu alloys. *Exp. Therm. Fluid. Sci.* **2010**, *34*, 1507–1516. [CrossRef]
26. Guo, J.D.; Wang, X.L.; Dai, W.B. Microstructure evolution in metals induced by high density electric current pulses. *Mater. Sci. Technol.* **2015**, *31*, 1545–1554. [CrossRef]
27. Qin, R.S.; Bhowmik, A. Computational thermodynamics in electric current metallurgy. *Mater. Sci. Technol.* **2015**, *31*, 1560–1563. [CrossRef]
28. Belov, N.A.; Akopyan, T.K.; Korotkova, N.O.; Timofeev, V.N.; Shurkin, P.K. Effect of cold rolling and annealing temperature on structure, hardness and electrical conductivity of rapidly solidified alloy of Al-Cu-Mn-Zr system. *Mater. Lett.* **2021**, *30*, 130199. [CrossRef]
29. Ada, P.; Cieslar, M.; Vostr, P.; Beva, F.; Prochazka, I. Electrical resistivity and positron lifetime studies of precipitation effects in Al-Cu alloy. *Acta Phys. Pol. A* **1995**, *88*, 111–117. [CrossRef]
30. Haslam, A.J.; Phillpot, S.R.; Wolf, D.; Moldovan, D.; Gleiter, H. Mechanisms of grain growth in nanocrystalline FCC metals by molecular-dynamics simulation. *Mater. Sci. Eng. A* **2001**, *318*, 293–312. [CrossRef]

31. Gupta, R.P. The electron wind force in electromigration. *J. Phys. Chem. Solids* **1986**, *47*, 1057–1066. [CrossRef]
32. Lodder, A. The driving force in electromigration. *Physica A* **1989**, *158*, 723–739. [CrossRef]
33. Kresse, T.; Borchers, C.; Kirchheim, R. Vacancy-carbon complexes in BCC iron: Correlation between carbon content, vacancy concentration and diffusion coefficient. *Scr. Mater.* **2013**, *69*, 690–693. [CrossRef]
34. Du, Y.; Chang, Y.A.; Huang, B.; Gong, W.; Jin, Z.; Xu, H.; Yuan, Z.; Liu, Y.; He, Y.; Xie, F.Y. Diffusion coefficients of some solutes in FCC and liquid Al: Critical evaluation and correlation. *Mater. Sci. Eng. A* **2003**, *363*, 140–151. [CrossRef]
35. Styles, M.J.; Marceau, R.K.W.; Bastow, T.J.; Brand, H.E.A.; Gibson, M.A.; Hutchinson, C.R. The competition between metastable and equilibrium S (Al_2CuMg) phase during the decomposition of Al-Cu-Mg alloys. *Acta Mater.* **2015**, *98*, 64–80. [CrossRef]
36. Fu, S.; Liu, H.; Qi, N.; Wang, B.; Jiang, Y.; Chen, Z.; Hu, T.; Yi, D. On the electrostatic potential assisted nucleation and growth of precipitates in Al-Cu alloy. *Scr. Mater.* **2018**, *150*, 13–17. [CrossRef]
37. Clementi, E.; Raimondi, D.L.; Reinhardt, W.P. Atomic screening constants from SCF functions. II. atoms with 37 to 86 electrons. *J. Chem. Phys.* **1967**, *47*, 1300–1307. [CrossRef]
38. Csiszar, G.; Misra, A.; Ungar, T. Burgers vector types and the dislocation structures in sputter-deposited Cu-Nb multilayers. *Mater. Sci. Eng. A* **2011**, *528*, 6887–6895. [CrossRef]
39. Brandt, R.; Neuer, G. Electrical resistivity and thermal conductivity of pure aluminum and aluminum alloys up to and above the melting temperature. *Int. J. Thermophys.* **2007**, *28*, 1429–1446. [CrossRef]
40. Fatmi, M.; Ghebouli, B.; Ghebouli, M.A.; Chihi, T.; Ouakdi, E.H.; Heiba, Z.A. Study of precipitation kinetics in Al-3.7wt% Cu alloy during non-isothermal and isothermal ageing. *Chin. J. Physiol.* **2013**, *51*, 1019–1032.
41. Ceresara, S.A. step annealing procedure for the determination of diffusion coefficients in metals by the resistometric method-application to the diffusion of Cu in Al. *Phys. Stat. Sol.* **1968**, *27*, 517–520. [CrossRef]
42. Chen, Z.; Zhao, Y.; Zhang, Z. Theoretical and experimental study of precipitation and coarsening kinetics of θ′ phase in Al-Cu alloy. *Vacuum* **2021**, *189*, 110263. [CrossRef]
43. Ho, C.Y.; Ackerman, M.W.; Wu, K.Y.; Havill, T.N.; Bogaard, R.H.; Matula, R.A.; Oh, S.G.; James, H.M. Electrical resistivity of ten selected binary alloy systems. *J. Phys. Chem. Ref. Data* **1983**, *12*, 183–322. [CrossRef]
44. Lalpoor, M.; Dzwonczyk, J.S.; Hort, N.; Offerman, S.E. Nucleation mechanism of $Mg_{17}Al_{12}$-precipitates in binary Mg-7wt.% Al alloy. *J. Alloys Compd.* **2013**, *557*, 73–76. [CrossRef]
45. Wu, Y.F.; Wang, M.P.; Li, Z.; Xia, F.Z.; Xia, C.D.; Lei, Q.; Yu, H.C. Effects of Pre-aging treatment on subsequent artificial aging characteristics of Al-3.95Cu-(1.32Mg)-0.52Mn-0.11Zr alloys. *J. Cent. South Univ.* **2015**, *22*, 1–7. [CrossRef]
46. Perez, M.; Dumont, M.; Acevedo-Reyes, D. Implementation of classical nucleation and growth theories for precipitation. *Acta Mater.* **2008**, *56*, 2119–2132. [CrossRef]
47. Du, Q.; Poole, W.J.; Wells, M.A. A mathematical model coupled to CALPHAD to predict precipitation kinetics for multicomponent aluminum alloys. *Acta Mater.* **2012**, *60*, 3830–3839. [CrossRef]
48. Holmedal, B.; Osmundsen, E.; Du, Q. Precipitation of non-spherical particles in aluminum alloys part I: Generalization of the Kampmann-Wagner numerical model. *Metall. Mater. Trans. A* **2016**, *47*, 581–588. [CrossRef]
49. Jiang, L.; Li, J.K.; Cheng, P.M.; Liu, G.; Wang, R.H.; Chen, B.A.; Zhang, J.Y.; Sun, J.; Yang, M.X.; Yang, G. Experiment and modeling of ultrafast precipitation in an ultrafine-grained Al-Cu-Sc alloy. *Mater. Sci. Eng. A* **2014**, *607*, 596–604. [CrossRef]
50. Qin, R.S.; Su, S.X.; Guo, J.D.; He, G.H.; Zhou, B.L. Suspension Effect of nanocrystalline grain growth under electropulsing. *Nanostruct. Mater.* **1998**, *10*, 71–76. [CrossRef]
51. Baldan, A. Review progress in Ostwald ripening theories and their applications to nickel-base superalloys part I: Ostwald ripening theories. *J. Mater. Sci.* **2002**, *37*, 2171–2202. [CrossRef]
52. Lifshitz, I.M.; Slyozov, V.V. The kinetics of precipitation from supersaturated solid solutions. *J. Phys. Chem. Solids* **1961**, *19*, 35–50. [CrossRef]
53. Streitenberger, P. Generalized Lifshitz-Slyozov Theory of grain and particle coarsening for arbitrary cut-off parameter. *Scr. Mater.* **1998**, *39*, 1719–1724. [CrossRef]
54. Philippe, T.; Voorhees, P.W. Ostwald ripening in multicomponent alloys. *Acta Mater.* **2013**, *61*, 4237–4244. [CrossRef]
55. Senkov, O.N. Particle size distributions during diffusion controlled growth and coarsening. *Scr. Mater.* **2008**, *59*, 171–174. [CrossRef]
56. Conrad, H. Effects of electric current on solid state phase transformations in metals. *Mater. Sci. Eng. A* **2000**, *287*, 227–237. [CrossRef]
57. Jiang, Y.; Tang, G.; Guan, L.; Wang, S.; Xu, Z.; Shek, C.; Zhu, Y. Effect of electropulsing treatment on solid solution behavior of an aged Mg alloy AZ61 strip. *J. Mater. Res.* **2008**, *23*, 2685–2691. [CrossRef]
58. Xiao, H.; Jiang, S.; Shi, C.; Zhang, L.; Lu, Z.; Jiang, J. Study on the microstructure evolution and mechanical properties of an Al-Mg-Li alloy aged by electropulsing assisted ageing processing. *Mater. Sci. Eng. A* **2019**, *756*, 442–454. [CrossRef]

Disclaimer/Publisher's Note: The statements, opinions and data contained in all publications are solely those of the individual author(s) and contributor(s) and not of MDPI and/or the editor(s). MDPI and/or the editor(s) disclaim responsibility for any injury to people or property resulting from any ideas, methods, instructions or products referred to in the content.